Supplementary Appendix 1

This appendix has been provided by the authors to give readers additional information about their work.

Supplement to: Gantner ML, Eade K, Wallace M, et al. Serine and lipid metabolism in macular disease and peripheral neuropathy. N Engl J Med. DOI: 10.1056/NEJMoa1815111

Supplemental Appendix

Table of Contents

Supplemental Materials and Methods

Study design and sampling:

HSAN1 patient recruitment

Our primary aim in examining HSAN1 patients was to test if MacTel is a comorbidity in HSAN1 patients beyond our proband family (Family 1). Patients with HSAN1 were recruited and enrolled between January 2018 and October 2018 to the MacTel registry. Inclusion criteria included ability to provide informed consent and confirmation of an HSAN1-causing mutation in the *SPTLC1* gene. Family 3 (SPTLC2 S384F) was already in the MacTel registry, previously having been examined and diagnosed with MacTel. Members of Family 2, P3 and P4 were recruited to visit their nearest MacTel registry site and/or assessed at the Moran Eye Institute for fasted serum collection and further imaging, including FLIO.

MacTel patient serum collection for metabolite analysis

Our primary aim in assessing metabolite levels in the MacTel cohort of 123 patients (Table S1) was to determine if deoxySLs were differentially abundant in MacTel patients without HSAN1-causing variants. Patient and control samples had previously been collected at three MacTel registry sites for metabolite studies. All samples available were measured and family members were excluded from the statistical analysis. The HSAN1 patients described above were not included in this study

Animal studies

For exploratory mouse studies we had 15 mice per diet, aiming to have mice available for 1) short term metabolite analysis in tissues, 2) longer term monitoring of phenotype presentation and 3) account for unexpected deaths or outliers. Based on the 24 hr plasma analysis for amino acids (from 5 mice) we estimated that n = 5 would be sufficient to assess plasma and tissue metabolite levels. We did not know ahead of time if, when and what phenotypes we would observe in the diet treated animals.

Clinical exams including FLIO:

Subjects' best-corrected visual acuities were recorded using standard ETDRS protocols, and retinal examinations were conducted after pupil dilation. All subjects were imaged with color fundus photography, fluorescein angiography, blue light reflectance, autofluorescence, and optical coherence tomography on a Heidelberg Spectralis confocal imaging system (Heidelberg, Germany). Subjects seen at the University of Utah had dual-wavelength autofluorescence macular pigment imaging and fluorescence lifetime imaging ophthalmoscopy (FLIO) on prototype instruments provided by Heidelberg Engineering[1]. FLIO images were initially read by the Moran Eye Center investigators who were not masked to the subjects' diagnoses. FLIO and all other patient images were then reviewed by the Moorfields Eye Hospital in a masked manner.

Genetic analyses:
Genomic DNA of MacTel patients and family members were analyzed with whole exome sequencing. Exome sequence was captured using SeqCap EZ Exome v3. Raw sequence data were quality-filtered with CASAVA (Illumina, Inc., San Diego, CA), and aligned to Human Reference Genome build hg19. Duplicates were removed with Dynamic Read Analysis for Genomics (Edico Genome, San Diego, CA) and variant calling was done according to best practices outlines in Genome Analysis Tool Kit (GATK v3.6) with variant selection using Variant quality Score Recalibration using HapMap v3.3, dbSNP, and 1000 genomes. The allele frequencies of all variants were compared to The Genome Aggregation Database (gnomAD) http://gnomad.broadinstitute.org/gene/ENSG00000198691;
accessed July 2018) and were filtered by minor allele frequency (MAF < 0.005), and consequence (missense, frameshift, splice donor/acceptor variants, and stop loss/gain). Functional annotation of variants was determined using computational software including Annovar using pathogenicity scores of MCAP, REVEL, Eigen, CADD, DANN, and SPIDEX. As a general guideline, pathogenic consequences are predicted for variants with scores over 0.025 for MCAP, 0.5 for REVEL, 0.5 for Eigen, 20 for CADD, 0.97 for DANN, and more than 2 or less than -2 for SPIDEX psi z-score.
All detected possibly disease-associated variants were confirmed by Sanger sequencing. Segregation of the variants with the disease was analyzed in all available family members according the dominant mode of inheritance as suggested from the family histories (Figure 1A, Figure S1).

Quantification of ellipsoid zone (EZ) loss in MacTel patients:
Participants' ellipsoid zone loss was quantified from high-density spectral domain optical coherence tomography (SD-OCT) retinal images as previously described[2]. Briefly, en-face images were generated from SD-OCT volume scans using the manufacturer's software (Heidelberg Eye Explorer, version 6.0.13.0, Heidelberg Engineering). Automatic segmentation, paired with manual correction, was used to generate an en face image of the EZ layer for each SD-OCT volume scan, which was viewed with the transverse display option in the 3D view panel. Manual correction of segmentation was important in the photoreceptor 1 segment line, which overlays the ellipsoid zone. Photoreceptor 1 was the reference line for the en face view, and the distance to the second line was set to 0. The color table option selected was "white on black." EZ loss was outlined in the en face image and the overlay was checked with each B-scan to confirm that the outline correctly demarcated the area of EZ loss, which was subsequently quantified when correspondence was achieved.

Serum collection for metabolite analysis:
Serum was collected from MacTel patients and gender and age matched controls. After overnight fasting, 5 ml of blood was collected in a clot activating vacutainer tube and immediately inverted to initiate clotting. After sitting at room temperature for 30 min blood was spun at 1200 g for 5 min, and serum was aliquoted into tubes, flash frozen and stored at -80°C. Two separate cohorts of patients/controls were recruited for this

study and samples were extracted and analyzed by mass spectrometry at two separate times. Results from these two cohorts were combined for statistical analysis.

Plasma sphingoid base extraction, hydrolysis and LCMS analysis:
Plasma sphingolipids were processed using a method adapted from Othman et al [3]. Briefly, 100 µL of plasma was mixed with 0.5 mL of methanol and spiked with internal standards, sphinganine d7, sphingosine d7 and deoxysphinganine d3 (Avanti lipids). The samples were placed on a mixer for 1 h at 37 °C, centrifuged @ 2800 g and the supernatant collected and acid hydrolyzed overnight at 65 °C with 75 µL of methanolic HCl (1N HCl,10M H_2O in methanol). Next, 100 µL of 10 M KOH was added to neutralize. 625 µL of chloroform, 100 µL of 2N NH_4OH and 500 µL of alkaline water were added, the sample vortex-mixed and centrifuged for 5 min at 16 000 g. The lower organic phase was washed three times with alkaline water and dried under air. LCMS analysis was performed on an Agilent 6460 QQQ LC-MS/MS. Metabolite separation was achieved with a C18 column (Luna 100 x 2.1 mm, 3 µm, Phenomenex). Mobile phase A was composed of a 60:40 ratio of methanol:water and mobile phase B consisted of 100% methanol with 0.1% formic acid with 5 mM ammonium formate added to both mobile phases. The gradient elution program consisted of holding at 40% B for 0.5 min, linearly increasing to 100% B over 15 min, and maintaining it for 9 min, followed by re-equilibration to the initial condition for 10 min. The capillary voltage was set to 3.5 kV, the drying gas temperature was 350 °C, the drying gas flow rate was 10 L/min, and the nebulizer pressure was 60 psi. Sphingoid bases were analyzed by SRM of the transition from precursor to product ions at associated optimized collision energies and fragmentor voltages (Table S11). Sphingoid bases were then quantified from spiked internal standards of known concentration and further verified via external standard curves.

Ceramide species determination:
Retinal organoids or 100 µL of plasma were extracted with 500 µL -20 °C methanol and 500 µL of ice-cold saline and spiked with d7 18:1/15:0 ceramide as internal control (Avanti lipids). An aliquot (50 µL) of homogenate was dried under air and resuspended in RIPA buffer for protein quantification using BCA assay (BCA Protein Assay, Lambda, Biotech Inc., US). To the remaining homogenate, 1 mL of chloroform was added and the samples were vortexed for 5 min followed by centrifugation at 4 °C for 5 min @ 15 000g. The organic phase was collected and 2 µL of formic acid was added to the remaining polar phase, which was re-extracted with 1 mL of chloroform. Combined organic phases were dried and the pellet was resuspended in 100 µL of buffer containing 100% methanol, 1 mM ammonium formate and 0.2% formic acid. Ceramide species were determined via liquid chromatography mass-spectrometry (Agilent 6460 QQQ). Ceramides were separated on C8 column (Spectra 3 µm C8SR 150 x 3mm ID, Peeke Scientific, CA) as previously described[4]. Mobile phase A was composed of 100% HPLC grade water containing 2 mM ammonium formate and 0.2% formic acid and mobile phase B consisted of 100% methanol containing 0.2% formic acid and 1 mM ammonium formate. The gradient elution program consisted of holding at 82% B for 3 min, up to 90% B over 1 min and linearly increasing to 99% B over 14 min maintaining it

for 7 min and down to 82% B over 2 min. The 82% mobile phase B was maintained for 3 min followed by re-equilibration for 10 min. The capillary voltage was set to 3.5 kV, the drying gas temperature was 350 °C, the drying gas flow rate was 10 L/min, and the nebulizer pressure was 60 psi. Ceramide species were analyzed by SRM of the transition from precursor to product ions at associated optimized collision energies and fragmentor voltages (Table S12). Ceramides were then quantified from spiked internal standard of known concentration.

Plasma amino acid extraction and GCMS analysis:
Plasma metabolites were extracted with a 9:1 MeOH:H_2O extraction containing an isotope labeled amino acid mix (Cambridge Isotope Laboratories, #MSK-A2-1.2) as internal standards. Following addition of extraction fluid, plasma was vortexed for 10 min followed by centrifugation for 10 min @ 16 000 g @ 4 °C. The supernatant was vacuum-dried at 4 °C and subsequently derivatized with 2% (w/v) methoxyamine hydrochloride (Thermo Scientific) in pyridine for 60 min following by 30 min sialyation N-tertbutyldimethylsilyl-N-methyltrifluoroacetamide (MTBSTFA) with 1% tert-butyldimethylchlorosilane (tBDMS) (Regis Technologies) at 37°C. Polar derivatives were analyzed by GC-MS using a DB-35MS column (30m x 0.25 mm i.d. x 0.25 µm, Agilent J&W Scientific) installed in an Agilent 7890A gas chromatograph (GC) interfaced with an Agilent 5975C mass spectrometer (MS) as previously described [5]. Plasma polar metabolite concentration was determined from labeled internal standards and corrected for natural isotope abundance using in-house algorithms adapted from [6].

Tissue metabolite extraction:
Frozen tissue samples (20-30 mg) were homogenized for 2 min using ceramic beads (Precellys 2 mL Hard Tissue Homogenizing Ceramic Beads Kit, Bertin Instruments, US) in 500 µL methanol and 500 µL saline containing sphingoid base and amino acid isotope labelled internal standards as detailed for plasma extraction above. An aliquot of homogenate (50 µL) was dried under air and resuspended in RIPA buffer for protein quantification using BCA assay (BCA Protein Assay, Lambda, Biotech Inc., US). To the remaining homogenate, 1 mL of chloroform was added and the samples were vortexed for 5 min followed by centrifugation at 4 °C for 5 min @ 15 000g. The organic phase was collected and 2 µL of formic acid was added to the remaining polar phase, which was re-extracted with 1 mL of chloroform. Combined organic phases were dried before hydrolysis and sphingoid base analysis as outlined for plasma above. Polar metabolites were quantified from the initial polar phase as described for plasma polar metabolite extraction.

Lipoprotein fractionation:
Donor serum was fractionated using a LDL/VLDL and HDL purification kit (Cell BioLabs, Inc) according to the manufacturer's protocol using serum pooled from four donors fasted overnight. Lipoprotein fractions were dialyzed and protein content measured by BCA.

Mouse husbandry and diet:
All animal procedures were approved by The Scripps Research Institute's Institutional Animal Care and Use Committee (IACUC) and we adhered to all federal animal experimental guidelines. Randomized male C57/Bl6J mice were started on amino acid adjusted diets at 8 weeks of age. Mice were fed ad libitum isocaloric and isonitrogenous control or serine and glycine free custom diets (Envigo Teklad Diets, Madison, WI) (Table S13). Average food consumption and mouse weights were monitored weekly.

For circadian plasma serine levels, blood was collected from mice fed the amino acid defined diets for two weeks. Plasma was collected with heparinized capillaries from tail bleeds every 4 hours starting at ZT 0, 6 am light onset.

For fasted plasma and tissue metabolite levels, food was removed in the morning and mice were fasted 6 hr prior to euthanization by brief isoflurane exposure and decapitation. Tissues were dissected rapidly and flash frozen in liquid N_2 prior to metabolite extraction.

Ganzfeld Electroretinography:
Mice were dark adapted overnight and all work was done under red light. Mice were anesthetized by intraperitoneal injection of 15 mg/kg ketamine and 7 mg/kg xylazine and pupil dilated with 1% tropicamide and 2.5% phenylephrine. Silver needle were used as a reference (central joules) and ground (skin above tail). Full-field ERGs were recorded in each eye using active contact lens electrodes (Mayo; Inazawa, Japan). Recordings were made using an electronically controlled Ganzfeld dome (Espion E2 with Colordome; Diagnosys; Westford, MA). Scotopic responses were performed in the dark with a series of white flashes of increasing intensities (0.01, 25 and 50 cd*s/m^2). Photopic response was measured after light-adaptation (30 cd/m^2 background) with a 25 cd*s/m^2 flash. Subsequently, flicker response was recorded from 10-Hz (25 cd*s/m^2) stimuli. ERG responses were filtered at 0.3-300 Hz and signal averaging applied.

EchoMRI:
The EchoMRI 3-in-1 instrument (EchoMRI LLC, Houston, TX) is a quantitative nuclear magnetic resonance (qNMR) imaging system for whole body composition analysis of unaesthesized small animals [7,8], and qNMR body composition analysis with EchoMRI instrumentation has been proposed to be "gold standard" methodology for metabolic studies in the mouse [9]. Following calibration, each mouse was placed in a holder and placed into the EchoMRI chamber and lean mass, fat mass and water mass were calculated in a masked fashion.

Hot plate test:
To examine thermal nociception (which requires circuitry in the brain as well as spinal cord), mice were placed in a glass cylinder on a 52-54 °C hot plate [10]. Latency to a nociceptive response (hind paw lick, flick, or jump) was measured, and mice were

immediately removed from the apparatus in a masked fashion. If a nociceptive response was not seen within 30 s, the test was stopped.

Retinal organoid generation and drug treatment:
The human induced pluripotent stem cell (hiPSC) line used was derived from peripheral blood mononuclear cells from a female. Reprogramming was performed by the Harvard iPS core facility using sendai virus for reprogramming factor delivery. All cell lines were obtained with verified normal karyotype and contamination-free. hiPSC were maintained on Matrigel (BD Biosciences) coated plates with mTeSR1 medium (STEMCELL Technologies). Cells were passaged every 3-4 days at approximately 80% confluence. Colonies containing clearly visible differentiated cells were marked and mechanically removed before passaging.
Retinal organoids were differentiated from hiPSCs between passage 10 and 20. Retinal organoids were initiated in differentiated as described in [11]. Following week 4 of differentiation organoids were cultured in rotating cell suspension until week 18. Mature retinal organoids were cultured in Retinal Differentiation Media plus 10% FBS, 100 µM Taurine, and 2 mM Glutamax starting at week 8 of differentiation. Fully mature retinal organoid tissue were assayed between 26 and 30 weeks post differentiation.

For lipid toxicity and rescue assays lipids and drugs were added to organoid culture media at concurrent times. Organoids were cultured in experimental conditions for 4 days with a condition specific media change at day 2. Lyophilized lipids, deoxy-sphinganine (Avanti 860493), deoxy-sphingosine (Avanti 860470), d14,15DB deoxy-sphingosine (1-deoxy-sphingosine(m18:1(14Z)) Cayman 24515), sphingosine (Avanti 860490), and sphinganine (Avanti 860498), were resuspended to stock concentrations at 5 mM in EtOH and subsequently added to retinal organoid culture media at experimentally specified concentrations. For control conditions equivalent amounts of EtOH were added to media. Drug rescue conditions included Fumonisin B1 (Sigma F1147) at 35 µM and Fenofibrate (Sigma F6020) at 20 µM. Organoids were subsequently fixed and processed for immunohistochemistry.

For analysis of sphingolipid/deoxy-sphingolipid subspecies enrichment following co-culture of organoids with resuspended lipids organoids were co-cultured with 1 µM of specified lipid for two days. Following the two day co-culture organoids were cleaned of any attached RPE clumps then rinsed with saline and snap frozen in liquid nitrogen before processing.

Immounohistochemistry:
Organoid tissue fixed in 4% PFA in PBS for 10 mins, washed in PBS, and then in 20% sucrose in PBS overnight. Tissues were embedded in O.C.T compound and frozen. Cryosectioning was done at 14 µm and slices were mounted on glass polylysine coated slides. Prior to primary antibodies samples were blocked with 5% donkey serum in PBS with 0.1% tween. Primary antibodies were added to samples at 4°C and incubated overnight. Following primary antibodies samples were washed 3 x 10 mins in PBS.

Secondary antibodies were added at room temp for 2 hours. Dapi was added at 1:1000 in PBS for 10 mins following secondary antibodies.
Primary antibodies: rabbit anti Recoverin (1:500, Millipore AB5585), mouse anti CRALBP (1:500, Abcam 15051), mouse anti Map2 (1:500, BD Bioscience 556320), mouse anti Rhodopsin (1:500, Millipore MAB5356), rabbit anti Peripherin2 (1:500, Proteintech 18109-1-ap)
Secondary antibodies: donkey anti rabbit alexafluor 555 (1:1000, Invitrogen 31572), donkey anti rabbit alexafluor 488 (1:1000, Invitrogen 21206), donkey anti mouse alexafluor 555 (1:1000, Invitrogen 31570), donkey anti mouse alexafluor 488 (1:1000, Invitrogen 21202).
Quantification of cell death in Photoreceptors: TUNEL staining was performed using In Situ Cell Death Detection Fluorecein kit (Sigma cat# 11684795910) prior to addition of anti-recoverin primary antibody. Overlapping Tunel positive staining and DAPI staining within a recoverin positive cell was counted as cell death within a photoreceptor. Cell death was normalized to the area of recoverin staining in the retinal organoid.

Statistical Analysis:

Animal studies
P values were calculated using a Student's two-tailed two sample t test, assuming equal variances, unless otherwise specified. In figures, P-value significance levels were indicated by * Benjamini-Hochberg corrected P value between 0.01 and 0.05; **, corrected P value between 0.001 and 0.01; ***, corrected P value <0.001. The longitudinal data was tested using mixed linear regression modeling where the mouse identifier was included as a random intercept. Correlation between metabolites abundances was calculated using pearson's correlation and tested for significance using linear modeling on log transformed abundances as performed for analyses using human subjects.

Cell studies
A square root transformation to cell death count per 10,000 was applied to transform the data to have an approximately normal distribution. The relationship between cell death and other factors was tested by regression of cell death count on factor levels using linear regression modeling.

Human targeted metabolite analysis
For human targeted metabolite analysis, samples were extracted, processed and analyzed by GCMS or LCMS in batches. A logarithmic transformation was applied to the metabolite abundances given their skewed distribution. EZ loss measurements were normalized by applying the square root transformation of the measured area. Given the logarithmic transformation applied to metabolites abundance, regression results are interpreted as change in percentage using the formula change (%)= (exp(b)-1)*100.

Human Deoxy-sphinganine and serine metabolite analysis
To investigate differences in deoxy-sphinganine and serine levels, we fitted mixed effects regression models including the batch factor as a random effect given the

imbalance between case and control numbers in each batch. For each model, we first estimated the effect of all available covariates on deoxy-sphinganines or serine. These included: gender, age, ethnicity, mass spectrometry batch, BMI, type 2 diabetes and sample collection site. Nominally non-significant covariates were then excluded from the final mixed effects regression model.

Human Deoxy-sphinganine correlation analysis
To investigate the correlation between deoxy-sphinganines and other metabolites, we analyse spearman rank correlation coefficients. We corrected for potential confounding effects of covariates and MacTel disease by applying a mixed model regression analysis which included all aforementioned covariates and MacTel status as fixed effects while deoxy-sphinganine batch was included as a random effect. Given that amino acids were extracted and analyzed separately to that of sphingoid bases, amino acids were corrected for batch effect through residualisation separately, prior to their inclusion in the regression modelling. Similarly, when amino acid metabolites were used as the dependent variable their batch was included as a random effect.

Human Deoxy-sphinganine and disease progression analysis
To investigate the effect of deoxy-sphinganines on disease progression we performed mixed modelling regression using only MacTel cases. We regressed deoxy-sphinganine levels on EZ loss while accounting for batch incorporating it as a random effect. Maximum EZ loss between right and left eye was used to describe the disease progression.

General specifications:
Descriptive studies were not tested for statistical significance. P-values from tests performed on the same dataset were corrected for multiple testing using Benjamini-hochberg correction. Regression results are presented as regression coefficient “b” represents magnitude of the effect of the factor of interested, “p*” represents nominal p-value and “p” represents multiple testing corrected p-value. P values of regression coeffiecients included in the model as covariates were not corrected for multiple testing and were not used to infer broader effect sizes. Benjamini-hochberg corrected p-values less than 0.05 were considered as statistically significant. EZ loss progression analysis was not corrected for multiple testing since a subset of the initial dataset was used (cases-only). For this reason, only estimates of effects and unadjusted 95% confidence intervals are presented. These estimates cannot be used to infer broader effects. Regression model assumptions and fit were assessed using residual diagnostics plots. Statistical analyses were performed using R Statistical Software (version 3.5.1) and IBM SPSS Statistics Version 25. Mixed linear modeling was performed using the package lme4[12] while inferential results were obtained using the package lmerTest[13].

Supplemental Figures

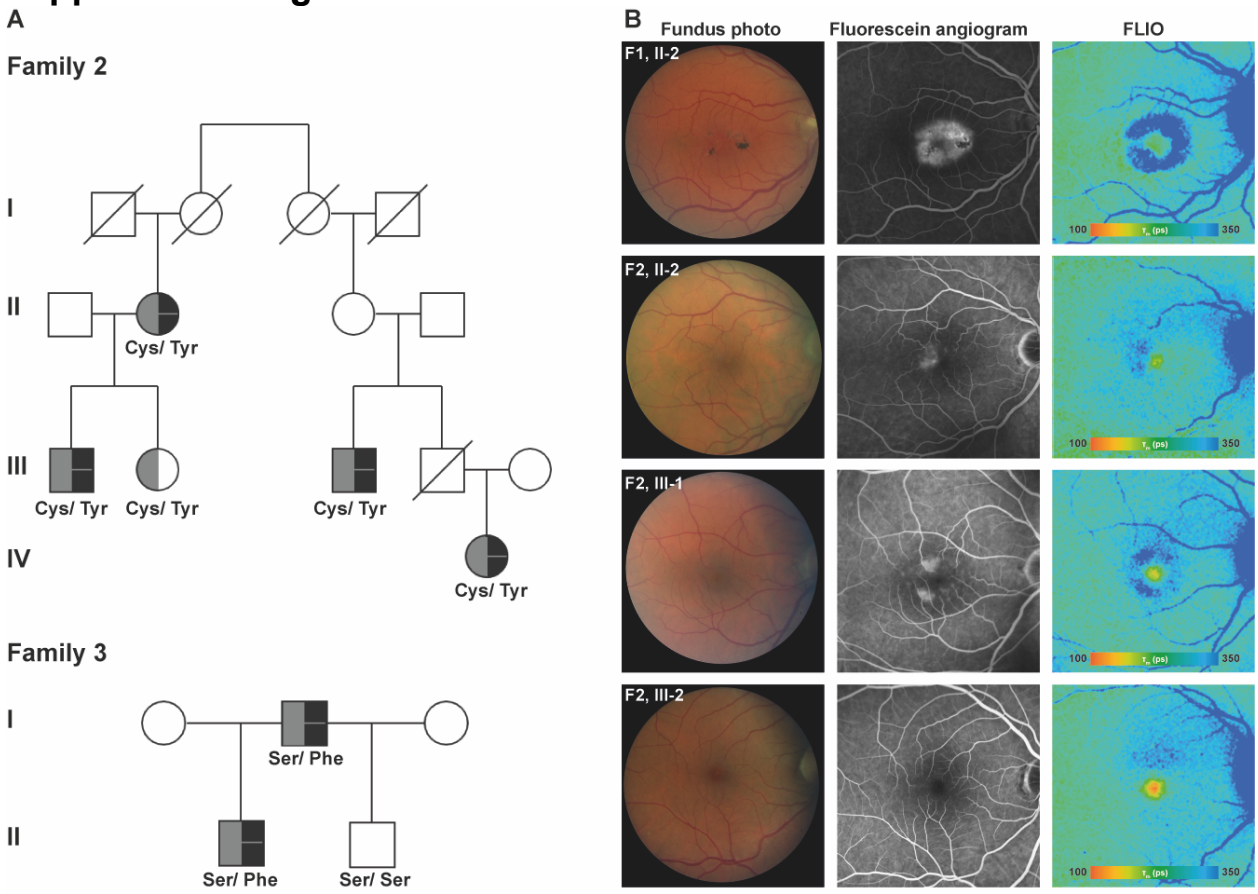

Figure S1. Additional family pedigrees and ophthalmological images from HSAN1 patients

A. Pedigrees of families 2 and 3. Affected individuals are indicated with filled symbols, unaffected with clear symbols. Black half-symbol indicates MacTel, grey indicates HSAN1A/C. Disease-causing mutation for, family 2 at SPTLC1 amino acid position 133, or family 3 at SPTLC2 position 384, are shown. All patients for whom SPTLC variants are presented were clinically examined. **B.** Ophthalmological images from selected patients highlighting MacTel-characteristic fundus color images (column 1), parafoveal late-phase fluorescein angiogram hyperfluorescence (column 2), and parafoveal blue rings of long FLIO lifetimes and loss of macular pigment (column 3) in all patients examined.

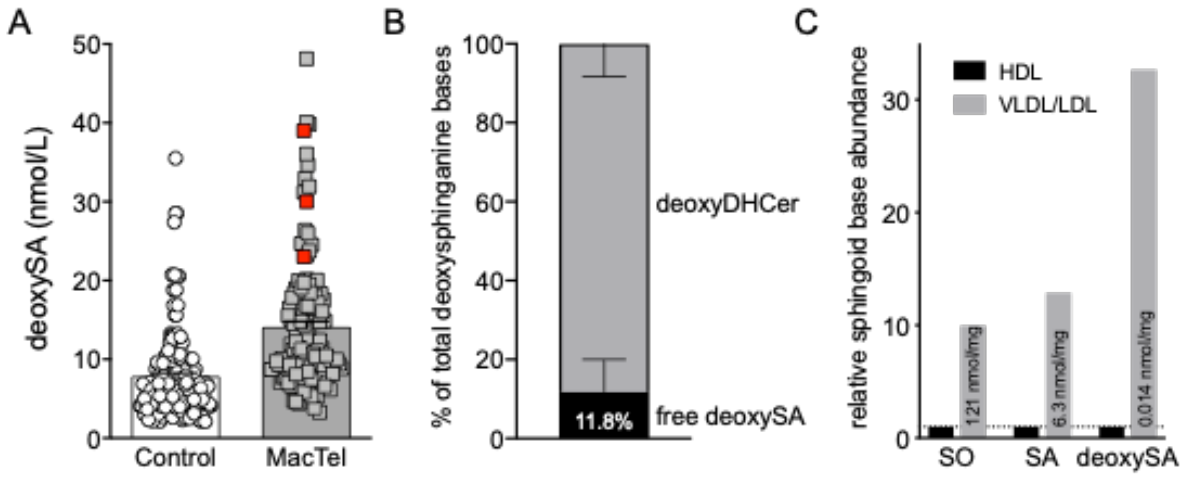

Figure S2. DeoxySAs are predominantly derived from deoxyDHCer species and found in VLDL/LDL fractions

A. DeoxySA levels including HSAN1 patients: red data points (F1, II-2, III-2, III-3), none of whom were taking serine (Table 1, Figure 1B). **B.** Free deoxySA and total hydrolyzed deoxySA were quantified and compared in fasted patient sera (n = 11). **C.** Relative abundance of hydrolyzed sphingoid bases in VLDL/LDL versus HDL fractions taken from fasted serum pooled from 4 control donors. Quantification of sphingoid base in VLDL/LDL fraction is indicated on bar normalized per mg of protein. These are descriptive studies without statistical analysis.

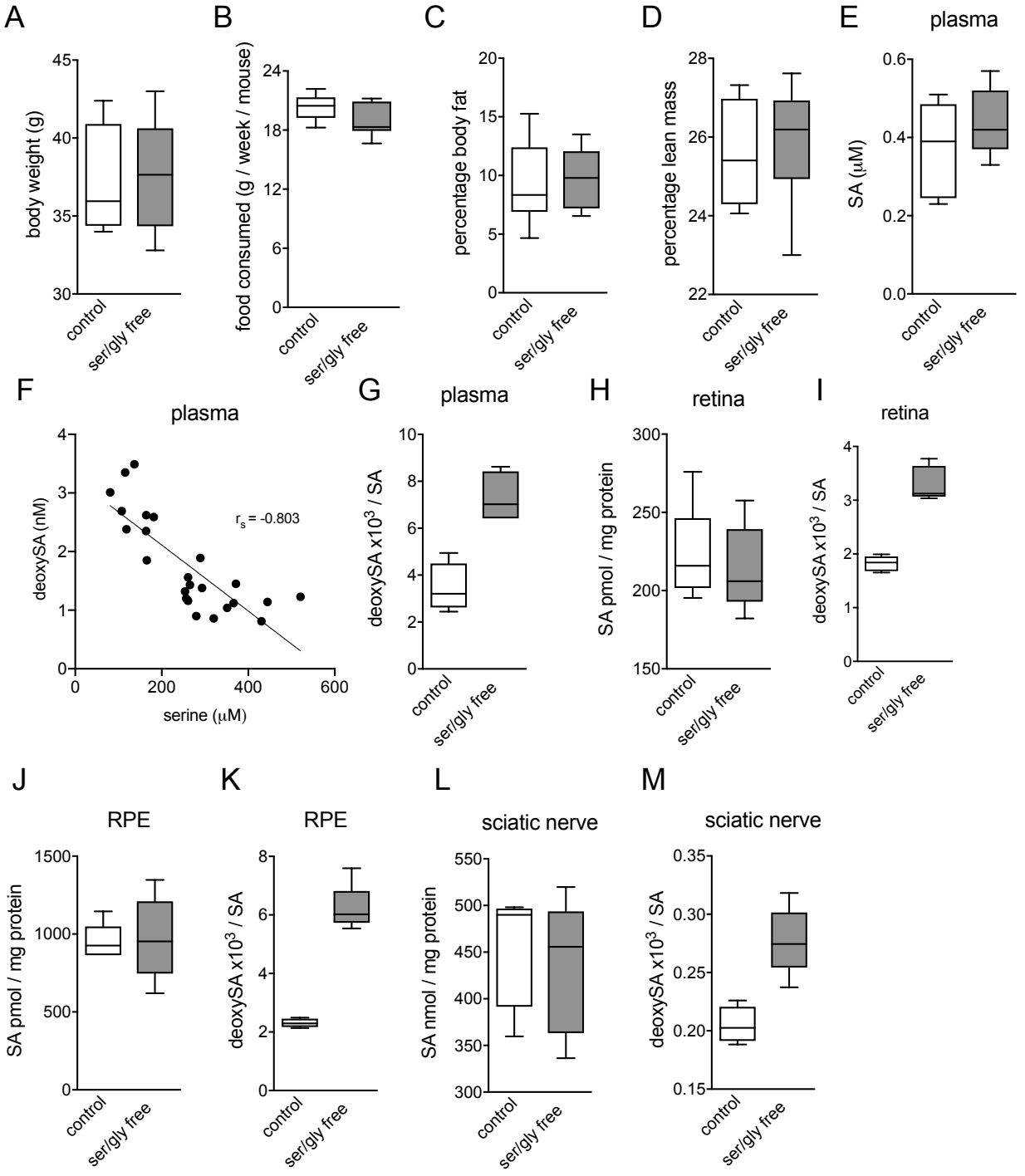

Figure S3. Additional analyses of mice fed serine/glycine-free or control diet
A. Body weight of mice after being fed control or serine/glycine-free diet for 10 months (n = 8). **B.** Average of 5 weeks food consumption per mouse per week on control or serine/glycine-free diet (n = 8). **C – D.** Percentage body fat (C) and lean mass (D) measured by echoMRI in mice fed control and serine free diet for 10 months (n = 8). **E.**

SA quantification in plasma in mice fed control and serine/glycine-free diet for 3 months (n = 5) **F.** Correlation between mouse plasma serine deoxySA tested using linear regression on log-transformed values. Outlier detection by regression model was performed on leverage distance presented in mode diagnostics plots. One mouse observation was deemed to be an outlier by the regression model and was discarded from this association testing. **G - M**. SA quantification and deoxySA/SA ratio in indicated tissues in mice fed control and serine/glycine-free diet for 3 months. SA levels are normalized to mg of protein extracted from sample after extraction (n = 5). Data represented by box and whiskers indicating median, first and third quartile and min and max values. These are descriptive studies without statistical analysis.

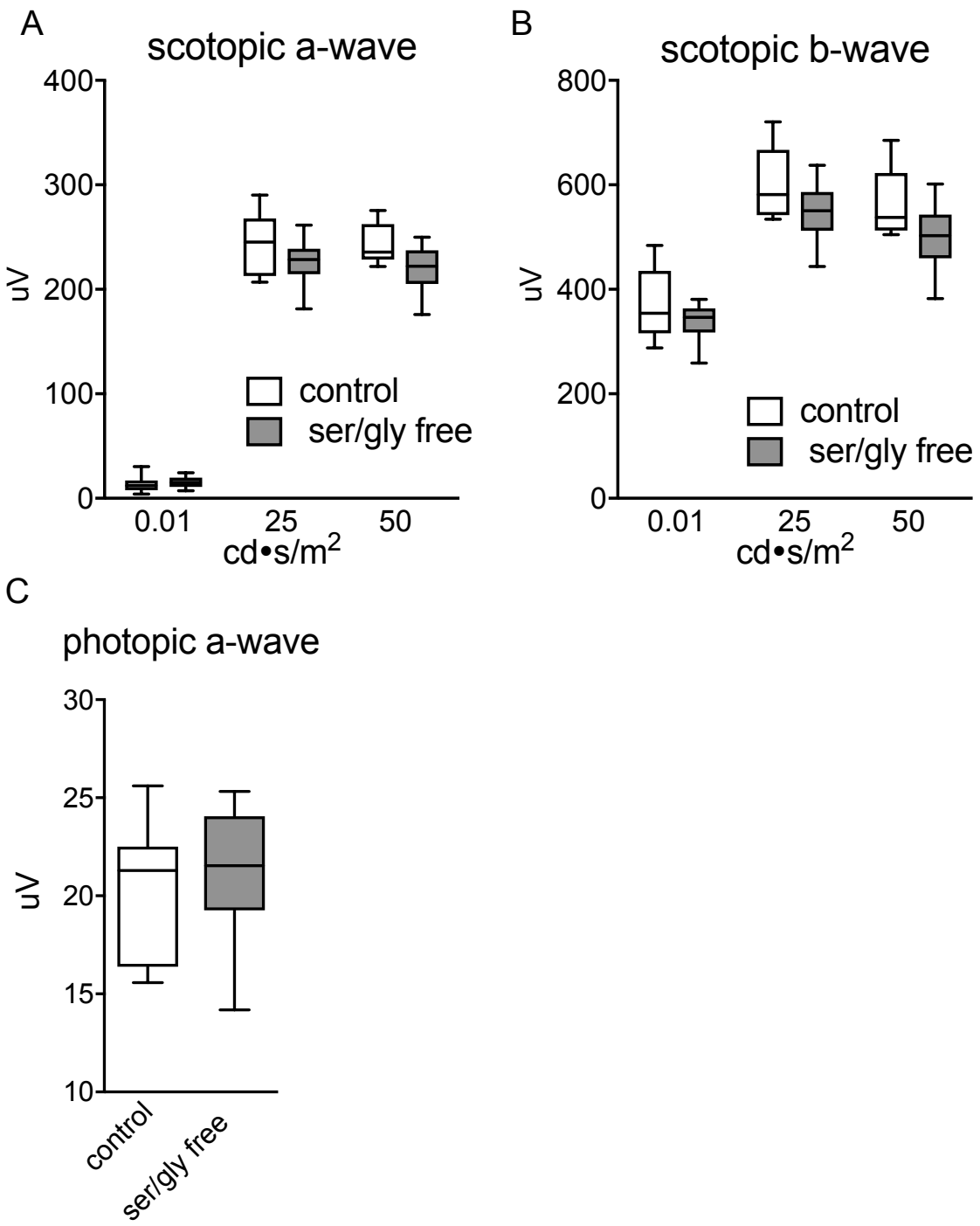

Figure S4. Additional effects of serine/glycine-free diet on electroretinograms in mice.

A – C. Indicated responses from electroretinography (ERG) in mice fed control or serine/glycine-free diet for 10 months. Scotopic a wave (A), scotopic b wave (B), and photopic a wave(C) (n = 8-10). Data represented by box and whiskers indicating median, first and third quartile and min and max values. These are descriptive studies without statistical analysis.

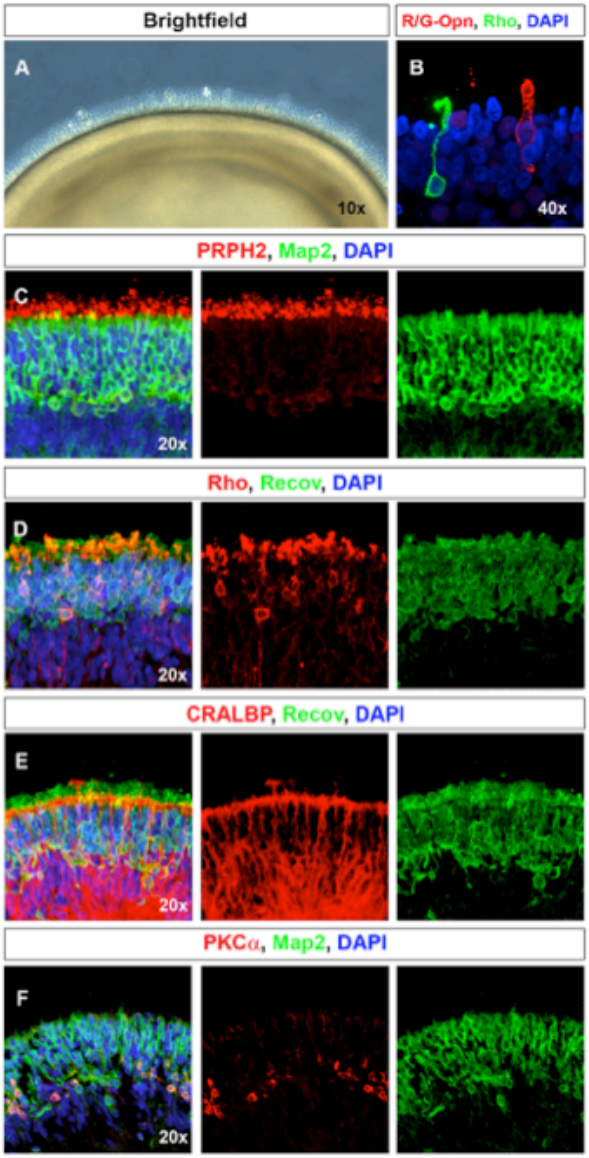

Figure S5. Immunohistochemical analysis of human retinal organoids.
A. Free floating retinal organoid tissue live in culture media viewed under bright field transillumination. Organoids have outer segments projecting out from the outer nuclear layer, multiple layers of neurons and glia, and a hollow central cavity. **B.** Confocal imaging showing both rods (α-rhodopsin, green) and cones (α-Red-green opsin, red) form in the outer nuclear layer with distinct morphology. **C-F.** Confocal images of cryosectioned retinal organoids showing photoreceptors (α-Map2 (Green, C and F), and α-Recoverin (Green, D and E)) polarized with outer segments (α-PRPH2, Red, C). **D.** Many of the photoreceptor are rods shown by strong expression of rhodopsin (α-Rhodopsin (Red)) in the outer segments and cell soma. **E.** Müller glia (α-CRALBP, red) reside in the inner nuclear layer just below the photoreceptors (α-Recoverin, green) and project processes with end feet into the photoreceptor layer. **F.** Bipolar neurons (α-PKCα, Red) reside in the inner nuclear layer just below the photoreceptor layer.

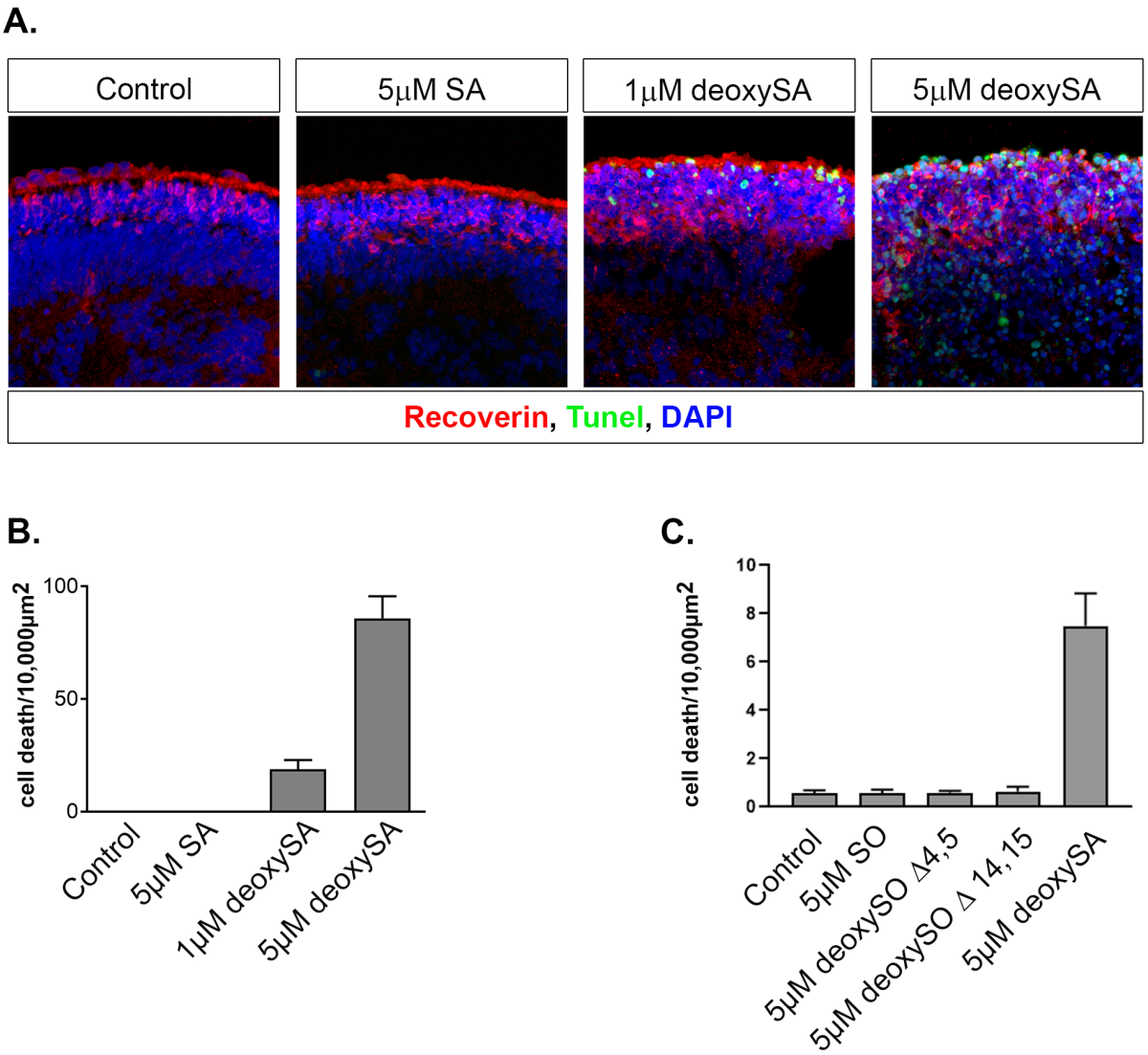

Figure S6. Deoxysphingolipid-induced cell death of photoreceptors in human retinal organoids.

A. Representative confocal images of cell death (Tunel, green) within the photoreceptors (recoverin, red) of the retinal organoid ONL after 4 days of treatment with either control media, 5 μM SA, 1 μM deoxySA, and 5 μM deoxySA. **B.** DeoxySA and not SA is toxic to photoreceptors. Quantification of cell death in human photoreceptors following treatment with control media, 5 μM SA, 1 μM deoxySA, and 5 μM deoxySA (n = 5 per group). **C.** Neither SO nor either form of deoxySO are toxic to photoreceptors. Quantification of cell death in human photoreceptors following treatment with control media (n=20), or 5 μM of either SO (n=14), deoxySO D4,5 (n=14), deoxySO D14,15 (n=14), or deoxySA. These are descriptive studies without statistical analysis.

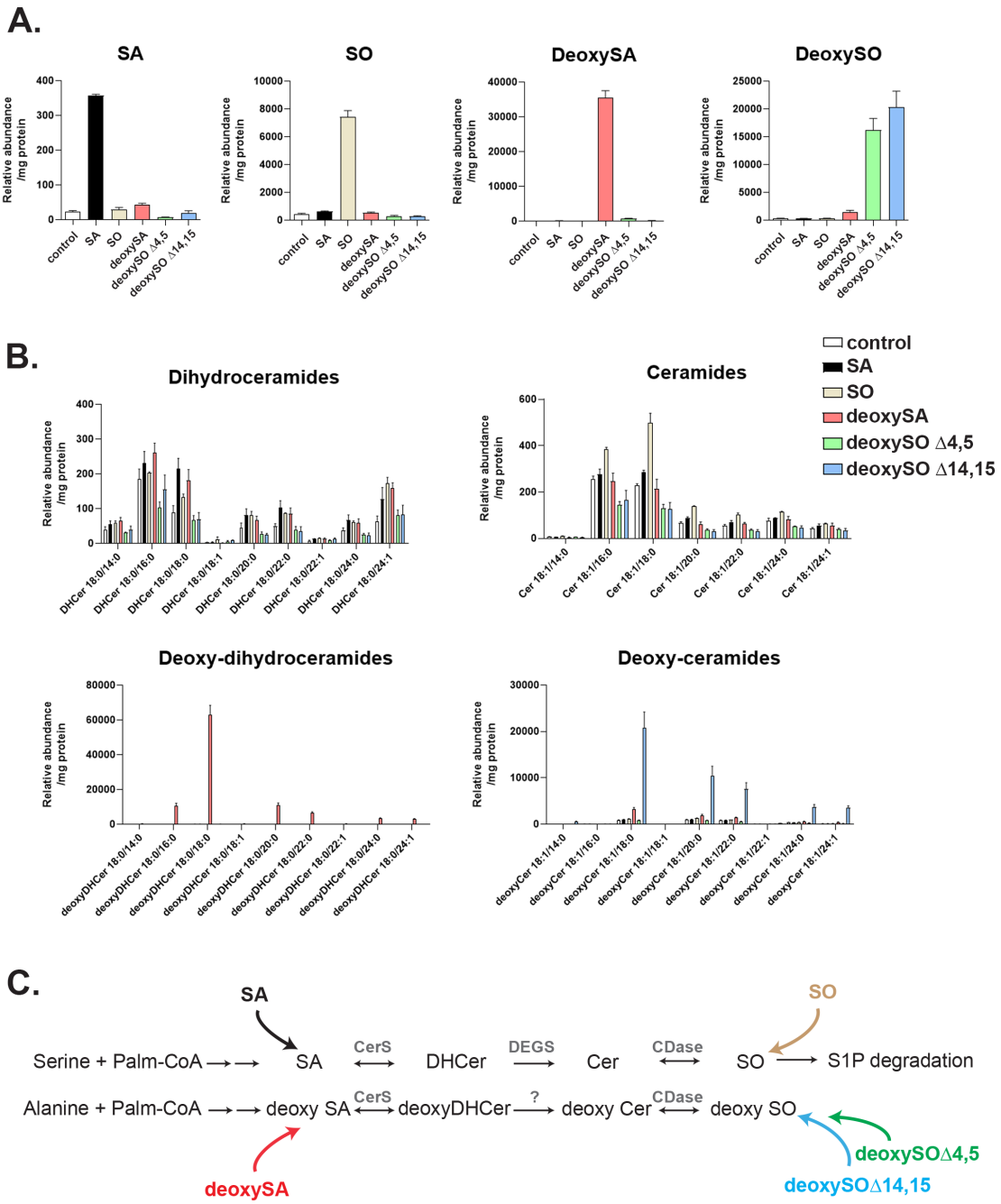

Figure S7. DeoxyDHCer is the neurotoxic deoxySL species.
A,B. Enrichment of deoxySL species following treatment with control media or 1μM of either SA, SO, deoxySOΔ4,5, deoxySOΔ14,15, or deoxySA for 2 days. n=3 replicates of 6 combined organoids for each SL treatment. Descriptive study without statistical analysis **A**. Measurements of SL species showing that organoids are enriched for the SL species that is added in their respective experimental conditions. **B.** Measurements of downstream SL/deoxySL metabolites with varying fatty acyl chain lengths following treatment with 1 μM SL/deoxySL. DeoxyDHCer subspecies are only enriched in

organoids treated with deoxySA. DeoxyCer subspecies are enriched in organoids treated with either deoxySA or deoxySOΔ14,15, with deoxySOΔ14,15having greater than 7 fold more enrichment than deoxySA. **C.** A schematic showing the directionality of enzymes in the deoxySL pathway. Addition of deoxySA can contribute to enrichment of pools of all deoxySLs, however, because of the unidirectional conversion of deoxyDHCer to deoxyCer, deoxySOs can only enrich pools of deoxyCer. These are descriptive studies without statistical analysis.

Supplemental Tables

Table S1. Demographics of patients used for plasma metabolite analysis.

	Control (n=94)	MacTel (n=125)
Female (n)	46 (49%)	67 (54%)
Age (avg ± stdev)	59 ± 10	63±9
BMI (avg ± stdev)	27 ± 5	29±6
Diabetes:		
Type 2 Diabetes	20 (21%)	43 (34%)
Unknown	7 (7%)	1 (0.8%)
Collection site:		
USA	43 (46%)	18 (14%)
UK	49 (52%)	97 (78%)
Australia	2 (2%)	10 (8%)
Ethnicity		
Caucasian	72 (77%)	92 (74%)
Other	22 (23%)	33 (26%)

Table S2. Results from mixed effects linear regression of MacTel on SA

Fixed Effects

	b	Std. Error	t	df	p*	p
(Intercept)	1.38	0.16	8.62	179	<2e-16	NA
Ethnicity	0.01	0.06	0.25	192	0.806	NA
Age	-0.01	0	-3.15	191	0.002	NA
Sex at birth	-0.12	0.05	-2.63	194	0.009	NA
Collection site Aus	-0.26	0.13	-1.98	86	0.051	NA
Collection site USA	-0.06	0.07	-0.92	100	0.36	NA
T2D status	-0.17	0.06	-3.01	196	0.003	NA
MacTel	0.04	0.06	0.71	126	0.476	0.476

Random Effects

	Std. Dev	n groups
SA Analytical batch	0.124	13
Residual	0.328	

p values calculated using Satterthwaite d.f.

T2D: Type 2 Diabetes

Table S3. Results from mixed effects linear regression of MacTel on deoxySA

Fixed Effects

	b	Std. Error	t	df	p*	p
(Intercept)	1.821	0.087	20.931	21.298	1.09e-15	NA
MacTel	0.611	0.086	7.125	175.187	2.61e-11	1.04e-10

Random Effects

	Std. Dev.	# groups
DeoxySA Analytical batch	0.200	13
Residual	0.523	

p values calculated using Satterthwaite d.f.

Table S4. Results from mixed effects linear regression of ellipsoid zone (EZ) loss on deoxySA levels.

Fixed Effects

	b	Std. Error	t	df	p*	p
(Intercept)	2.355	0.093	25.382	28.044	<2e-16	NA
EZ max	0.148	0.073	2.018	113.929	0.045	NA

Random Effects

	Std. Dev.	# groups
DeoxySA Analytical batch	0.155	12
Residual	0.504	

p values calculated using Satterthwaite d.f.

EZ max: Maximum ellipsoid zone in each patient (similar results were observed when the average EZ lesion between eyes was used).

Table S5. Results from mixed effects linear regression of MacTel and T2D on deoxySA

Fixed Effects

	b	Std. Error	t	df	p*	p
(Intercept)	1.841	0.095	19.382	25.582	< 2e-16	NA
MacTel	0.516	0.097	5.229	181.278	4.67e-07	9.33e-07
T2D	-0.116	0.139	-0.831	206.998	0.407	4.652
MacTel*T2D	0.328	0.170	1.932	206.143	0.055	0.073

Random Effects

	Std. Dev.	# groups
DeoxySA Analytical batch	0.206	13
Residual	0.514	

p values calculated using Satterthwaite d.f.

T2D: Type 2 Diabetes

Table S6. Results from mixed effects linear regression of MacTel on serine

Fixed Effects

	b	Std. Error	t	df	p*	p
(Intercept)	4.832	0.082	58.892	4.438	1.36e-07	NA
MacTel	-0.231	0.035	-6.641	215.946	2.49e-10	6.63e-10

Random Effects

	Std. Dev.	# groups
Serine Analytical batch	0.173	5
Residual	0.229	

p values calculated using Satterthwaite d.f.

Table S7. Explorative spearman correlation analysis of metabolite levels in MacTel samples.

	age	BMI	dSA	SA	Met	Lys	Ala	Val	Leu	Ile	Ser	Phe	Asp	Pro	Glu	Tyr
age	1.00	-0.06	0.03	-0.22	-0.08	-0.02	0.02	-0.09	-0.12	-0.09	0.06	-0.06	-0.01	-0.05	-0.02	-0.05
BMI	-0.06	1.00	0.10	-0.01	-0.06	0.06	0.02	0.13	0.10	0.16	-0.16	0.05	-0.06	0.13	0.19	0.14
dSA	0.03	0.10	1.00	0.20	0.20	0.17	0.28	0.26	0.25	0.24	-0.21	0.26	0.14	0.35	0.24	0.06
SA	-0.22	-0.01	0.20	1.00	0.08	0.07	-0.06	0.11	0.13	0.13	0.10	0.13	0.14	0.00	0.15	0.07
Met	-0.08	-0.06	0.20	0.08	1.00	0.78	0.62	0.76	0.79	0.74	0.57	0.81	0.42	0.61	0.31	0.74
Lys	-0.02	0.06	0.17	0.07	0.78	1.00	0.62	0.77	0.75	0.68	0.46	0.76	0.44	0.52	0.29	0.69
Ala	0.02	0.02	0.28	-0.06	0.62	0.62	1.00	0.65	0.61	0.60	0.46	0.64	0.45	0.70	0.44	0.46
Val	-0.09	0.13	0.26	0.11	0.76	0.77	0.65	1.00	0.96	0.94	0.44	0.82	0.45	0.70	0.52	0.71
Leu	-0.12	0.10	0.25	0.13	0.79	0.75	0.61	0.96	1.00	0.96	0.43	0.83	0.43	0.70	0.49	0.70
Ile	-0.09	0.16	0.24	0.13	0.74	0.68	0.60	0.94	0.96	1.00	0.41	0.77	0.38	0.71	0.50	0.67
Ser	0.06	-0.16	-0.21	0.10	0.57	0.46	0.46	0.44	0.43	0.41	1.00	0.51	0.54	0.38	0.30	0.48
Phe	-0.06	0.05	0.26	0.13	0.81	0.76	0.64	0.82	0.83	0.77	0.51	1.00	0.59	0.63	0.47	0.78
Asp	-0.01	-0.06	0.14	0.14	0.42	0.44	0.45	0.45	0.43	0.38	0.54	0.59	1.00	0.37	0.46	0.46
Pro	-0.05	0.13	0.35	0.00	0.61	0.52	0.70	0.70	0.70	0.71	0.38	0.63	0.37	1.00	0.54	0.47
Glu	-0.02	0.19	0.24	0.15	0.31	0.29	0.44	0.52	0.49	0.50	0.30	0.47	0.46	0.54	1.00	0.40
Tyr	-0.05	0.14	0.06	0.07	0.74	0.69	0.46	0.71	0.70	0.67	0.48	0.78	0.46	0.47	0.40	1.00

n = 125 for all variables except BMI n = 123

dSA: deoxysphinganine

Table S8. Explorative spearman correlation analysis of metabolite levels in Control samples.

	age	BMI	dSA	SA	Met	Lys	Ala	Val	Leu	Ile	Ser	Phe	Asp	Pro	Glu	Tyr
age	1.00	-0.11	0.00	-0.28	0.15	0.09	0.26	0.01	-0.03	0.03	0.15	0.12	0.08	0.20	0.24	0.15
BMI	-0.11	1.00	0.16	-0.07	0.02	-0.04	0.18	0.00	-0.01	0.05	0.03	0.07	0.10	0.13	0.28	0.14
dSA	0.00	0.16	1.00	0.22	0.08	0.01	0.39	0.20	0.24	0.32	-0.48	0.05	-0.10	0.25	0.16	0.18
SA	-0.28	-0.07	0.22	1.00	-0.30	-0.20	-0.16	-0.17	-0.19	-0.17	-0.29	-0.20	-0.01	-0.25	-0.05	0.06
Met	0.15	0.02	0.08	-0.30	1.00	0.75	0.62	0.62	0.60	0.56	0.57	0.75	0.39	0.60	0.28	0.69
Lys	0.09	-0.04	0.01	-0.20	0.75	1.00	0.47	0.63	0.61	0.53	0.59	0.76	0.49	0.43	0.29	0.59
Ala	0.26	0.18	0.39	-0.16	0.62	0.47	1.00	0.33	0.31	0.35	0.25	0.48	0.38	0.52	0.33	0.48
Val	0.01	0.00	0.20	-0.17	0.62	0.63	0.33	1.00	0.94	0.88	0.30	0.69	0.23	0.51	0.34	0.52
Leu	-0.03	-0.01	0.24	-0.19	0.60	0.61	0.31	0.94	1.00	0.93	0.25	0.67	0.24	0.48	0.36	0.48
Ile	0.03	0.05	0.32	-0.17	0.56	0.53	0.35	0.88	0.93	1.00	0.11	0.57	0.15	0.51	0.32	0.49
Ser	0.15	0.03	-0.48	-0.29	0.57	0.59	0.25	0.30	0.25	0.11	1.00	0.47	0.44	0.22	0.23	0.28
Phe	0.12	0.07	0.05	-0.20	0.75	0.76	0.48	0.69	0.67	0.57	0.47	1.00	0.49	0.49	0.42	0.69
Asp	0.08	0.10	-0.10	-0.01	0.39	0.49	0.38	0.23	0.24	0.15	0.44	0.49	1.00	0.18	0.43	0.39
Pro	0.20	0.13	0.25	-0.25	0.60	0.43	0.52	0.51	0.48	0.51	0.22	0.49	0.18	1.00	0.38	0.57
Glu	0.24	0.28	0.16	-0.05	0.28	0.29	0.33	0.34	0.36	0.32	0.23	0.42	0.43	0.38	1.00	0.40
Tyr	0.15	0.14	0.18	0.06	0.69	0.59	0.48	0.52	0.48	0.49	0.28	0.69	0.39	0.57	0.40	1.00

n = 93 for all variables except; age, deoxy, and SA, n = 94, BMI n = 76
dSA: deoxySA

Table S9. Results from mixed effects linear regression of MacTel and serin on deoxySA levels.

Fixed Effects

	b	Std. Error	t	df	p*	p
(Intercept)	7.854	0.623	12.601	213.354	< 2e-16	NA
MacTel	0.317	0.079	4.029	206.789	7.84e-05	NA
Serine	-1.277	0.130	-9.797	208.632	< 2e-16	5.55e-18

Random Effects

	Std. Dev.	# groups
DeoxySA Analytical batch	0.233	13
Residual	0.430	

p values calculated using Satterthwaite d.f.

Table S10. Results from mixed effects linear regression of MacTel and alanine on deoxySA levels.

Fixed Effects

	b	Std. Error	t	df	p*	p
(Intercept)	-1.967	0.915	-2.150	213.654	0.033	NA
MacTel	0.528	0.085	6.225	169.684	3.66e-09	NA
Alanine	0.636	0.153	4.153	213.131	4.75e-05	7.59e-05

Random Effects

	Std. Dev.	# groups
DeoxySA Analytical batch	0.189	13
Residual	0.503	

p values calculated using Satterthwaite d.f.

Table S11. Mass spectrometer parameters for sphingoid bases

Sphingoid base	Parent	Daughter	CE
d18:0 SA	302.3	284.4	9
d18:0 SA d7	309.4	291.5	9
m18:0 deoxySA	286.3	268.5	13
m18:0 deoxySA d3	289.3	271.5	13

CE: collision energy

Table S12. Transition for ceramide assay

Sphingolipid species	Parent	Daughter	CE
DHCer 18:0/14:0	512.4	494.4	21
DHCer 18:0/16:0	540.4	522.4	21
DHCer 18:0/18:0	568.4	550.4	21
DHCer 18:0/18:1	566.4	548.4	21
DHCer 18:0/20:0	596.4	578.4	21
DHCer 18:0/22:0	624.4	606.4	21
DHCer 18:0/22:1	622.4	604.4	21
DHCer 18:0/24:0	652.4	634.4	21
DHCer 18:0/24:1	650.4	632.4	21
Cer 18:1/14:0	510.4	264.4	21
Cer 18:1/16:0	538.4	264.4	21
Cer 18:1/18:0	566.4	264.4	21
Cer 18:1/20:0	594.4	264.4	21
Cer 18:1/22:0	622.4	264.4	21
Cer 18:1/24:0	650.4	264.4	21
Cer 18:1/24:1	648.4	264.4	21
Deoxy-DHCer 18:0/14:0	496.7	268.4	21
Deoxy-DHCer 18:0/16:0	524.7	268.4	21
Deoxy-DHCer 18:0/18:0	552.7	268.4	21
Deoxy-DHCer 18:0/18:1	550.7	268.4	21
Deoxy-DHCer 18:0/20:0	580.7	268.4	21
Deoxy-DHCer 18:0/22:0	608.7	268.4	21
Deoxy-DHCer 18:0/22:1	606.7	268.4	21
Deoxy-DHCer 18:0/24:0	636.7	268.4	21
Deoxy-DHCer 18:0/24:1	634.7	268.4	21
Deoxy-Cer 18:1/14:0	494.4	266.4	21
Deoxy-Cer 18:1/16:0	522.4	266.4	21
Deoxy-Cer 18:1/18:0	550.4	266.4	21
Deoxy-Cer 18:1/18:1	548.4	266.4	21
Deoxy-Cer 18:1/20:0	578.4	266.4	21
Deoxy-Cer 18:1/22:0	606.4	266.4	21
Deoxy-Cer 18:1/22:1	604.4	266.4	21
Deoxy-Cer 18:1/24:0	634.4	266.4	21
Deoxy-Cer 18:1/24:1	632.4	266.4	21
SA 18:0	302.4	284.4	21
SO 18:1	300.4	282.4	21
doxSA m18:0	286.4	264.4	21
doxSO m18:1	284.4	266.4	21

Table S13. Composition of murine diets

Formula	Control (g/Kg)	Ser/gly-free (g/Kg)
L-Alanine	3.5	6.123
L-Arginine HCl	12.1	12.1
L-Asparagine	6	10.496
L-Aspartic Acid	3.5	6.123
L-Cystine	3.5	3.5
L-Glutamic Acid	40	69.976
Glycine	23.3	--
L-Histidine HCl, monohydrate	4.5	4.5
L-Isoleucine	8	8
L-Leucine	12	12
L-Lysine HCl	18	18
L-Methionine	8.2	8.2
L-Phenylalanine	7.5	7.5
L-Proline	3.5	6.123
L-Serine	3.5	--
L-Threonine	8.2	8.2
L-Tryptophan	1.8	1.8
L-Tyrosine	5	5
L-Valine	8	8
Sucrose	100	100
Corn Starch	381.2	365.539
Maltodextrin	150	150
Soybean Oil	80	80
Cellulose	50	50
Mineral Mix, AIN-93M-MX (94049)	35	35
Calcium Phosphate, monobasic, monohydrate	8.2	8.2
Vitamin Mix, AIN-93-VX (94047)	13	13
Choline Bitrartrate	2.5	2.5
TBHQ, antioxidant	0.02	0.02
	% by weight (% kcal)	
Protein	15.4(16.4)	15.4(16.6)
CHO	60.6 (64.5)	59.1 (63.9)
Fat	8 (19.2)	8 (19.5)
Kcal/g	3.8	3.7

Table S14. Statistical analysis of deoxySA levels in mice

type	p*	p
Plasma	0.001221	0.002443
Retina	0.000112	0.000448
RPE	0.004381	0.005841
Sciatic nerve	0.040162	0.040162

p value corrected for multiple testing reported in text, p* is the uncorrected value

Table S15. Statistical analysis of mouse phenotypes

type	p*	p
Photopic b wave	0.000568	0.00170399
Photopic flicker	0.00447267	0.00524514
Hot plate	0.00524514	0.00524514

p value corrected for multiple testing reported in text, p* is the uncorrected value

Table S16. Statistical analysis of deoxySA dose response in retinal organoids

	b	SE	t	p*	p
(Intercept)	0.58	0.15	3.94	0.00032	NA
DeoxySA_f5 vs f0	-0.15	0.21	-0.74	0.46592	4.66E-01
DeoxySA _f50 vs f0	0.51	0.21	2.41	0.02054	2.74E-02
DeoxySA _f500 vs f0	1.38	0.21	6.61	6.65E-08	1.33E-07
DeoxySA _f1000 vs f0	2.14	0.21	10.23	1.00E-12	4.00E-12

Table S17. Statistical analysis of treatment rescue in retinal organoids

	b	SE	t	p*	p
(Intercept)	3.64	0.15	24.11	< 2e-16	NA
Control vs dSA	-3.27	0.33	-10.03	3.37E-14	5.06E-14
dSA + Feno vs dSA	-2.07	0.22	-9.57	1.85E-13	1.85E-13
dSA + Fumo vs dSA	-2.99	0.25	-11.78	< 2e-16	6.00E-16

References

1 Sauer, L., Gensure, R. H., Hammer, M. & Bernstein, P. S. Fluorescence Lifetime Imaging Ophthalmoscopy: A Novel Way to Assess Macular Telangiectasia Type 2. *Ophthalmology. Retina* **2**, 587-598, doi:10.1016/j.oret.2017.10.008 (2018).

2 Heeren, T. F. C. *et al.* LONGITUDINAL CORRELATION OF ELLIPSOID ZONE LOSS AND FUNCTIONAL LOSS IN MACULAR TELANGIECTASIA TYPE 2. *Retina (Philadelphia, Pa.)* **38 Suppl 1**, S20-S26, doi:10.1097/iae.0000000000001715 (2018).

3 Othman, A. *et al.* Plasma 1-deoxysphingolipids are predictive biomarkers for type 2 diabetes mellitus. *BMJ open diabetes research & care* **3**, e000073, doi:10.1136/bmjdrc-2014-000073 (2015).

4 Bielawski, J. *et al.* Comprehensive quantitative analysis of bioactive sphingolipids by high-performance liquid chromatography-tandem mass spectrometry. *Methods in molecular biology (Clifton, N.J.)* **579**, 443-467, doi:10.1007/978-1-60761-322-0_22 (2009).

5 Vacanti, N. M. *et al.* Regulation of substrate utilization by the mitochondrial pyruvate carrier. *Molecular cell* **56**, 425-435, doi:10.1016/j.molcel.2014.09.024 (2014).

6 Fernandez, C. A., Des Rosiers, C., Previs, S. F., David, F. & Brunengraber, H. Correction of 13C mass isotopomer distributions for natural stable isotope abundance. *Journal of mass spectrometry : JMS* **31**, 255-262, doi:10.1002/(sici)1096-9888(199603)31:3<255::aid-jms290>3.0.co;2-3 (1996).

7 Taicher, G. Z., Tinsley, F. C., Reiderman, A. & Heiman, M. L. Quantitative magnetic resonance (QMR) method for bone and whole-body-composition analysis. *Analytical and bioanalytical chemistry* **377**, 990-1002, doi:10.1007/s00216-003-2224-3 (2003).

8 Tinsley, F. C., Taicher, G. Z. & Heiman, M. L. Evaluation of a quantitative magnetic resonance method for mouse whole body composition analysis. *Obesity research* **12**, 150-160, doi:10.1038/oby.2004.20 (2004).

9 Champy, M., Argmann, C., Chambon, P. & Auwerx, J. in *Standards of Mouse Model Phenotyping* Ch. 5, (2006).

10 Bannon, A. W. & Malmberg, A. B. Models of nociception: hot-plate, tail-flick, and formalin tests in rodents. *Current protocols in neuroscience* **Chapter 8**, Unit 8 9, doi:10.1002/0471142301.ns0809s41 (2007).

11 Ohlemacher, S. K., Iglesias, C. L., Sridhar, A., Gamm, D. M. & Meyer, J. S. Generation of highly enriched populations of optic vesicle-like retinal cells from human pluripotent stem cells. *Current protocols in stem cell biology* **32**, 1H 8 1-20, doi:10.1002/9780470151808.sc01h08s32 (2015).

12 Hammad, S. M. *et al.* Blood sphingolipidomics in healthy humans: impact of sample collection methodology. *Journal of lipid research* **51**, 3074-3087, doi:10.1194/jlr.D008532 (2010).

13 Kuznetsova A, B. P., Christensen RHB. ImerTest Package: Tests in Linear Mixed Effects Models. *Journal of Statistical Software* **82**, 1-26, doi:10.18637/jss.v082.i13 (2017).